Pol. J. Environ. Stud. Vol. XX, No. X (XXXX), 1-14
DOI: *10.15244/pjoes/219358* ONLINE PUBLICATION DATE: 2026-07-02

Original Research

Comprehensive Assessment of the Impacts of Expressway Construction on Forest Carbon Sink–Source Dynamics in Karst Regions

Qiongyao Ye[1], Lu Zhang[2, 3], Fen Huang[2, 3]°*, Mingzhu Fan[4], Qiong Xiao[2, 3], Qiang Zhang[2, 3]

[1]Guangxi Communications Design Group Co. Ltd, Nanning, 530029, China
[2]Institute of Karst Geology, CAGS/ Key Laboratory of Karst Dynamics, MNR&Guangxi / International Research Centre on Karst, UNESCO, Guilin, 541004, China
[3]Pingguo Guangxi, Karst Ecosystem, National Observation and Research Station, Pingguo, 531406, China
[4]Yulin Normal University, Yulin, 537000, China

Received: 16 October 2025
Accepted: 15 March 2026

Abstract

This study assessed the impacts of expressway construction on the carbon sink function of forest ecosystems in the karst region along the Du'an-Bama expressway in Guangxi, China. Field investigations, soil physicochemical measurements, biomass and carbon stock estimations, soil CO_2 flux monitoring, and greening project data analysis were conducted to characterize the carbon sink performance of different vegetation types and the changes induced by expressway construction. Results showed significant variations in biomass and carbon stock among vegetation types, with forests exhibiting the highest carbon sequestration capacity, followed by shrublands and grasslands. Soil physicochemical properties under different vegetation types also played an important role in determining carbon stock potential. The expressway project permanently occupied 217.22 hm^2 of land, leading to a biomass loss of 10207.21 t and a carbon stock reduction of 4601.89 tC. The implemented greening measures compensated for 993.30 t of biomass and 441.90 tC of carbon, corresponding to recovery rates of 9.73% and 9.60%, respectively. When considering the annual sequestration capacity of restored vegetation together with the reduction in soil CO_2 emissions beneath paved surfaces, the system exhibited an annual net carbon gain of 1629.65 tC, suggesting that the losses caused by permanent land occupation could be offset within approximately 2.6 years under the accounting framework of this study.

Keywords: expressway construction, karst region, forest carbon sink, biomass, carbon stock

*e-mail: huangfen@mail.cgs.gov.cn
°ORCID iD: 0000-0002-8833-873X

Introduction

With the intensification of global warming, the monitoring and assessment of forest ecosystem carbon stocks have become a central focus in ecological and environmental research [1-3]. Forest ecosystems constitute a vital component of the terrestrial carbon cycle [4, 5]. Through photosynthesis, forests sequester atmospheric CO_2 into vegetation and soils, thereby mitigating the rise in greenhouse gas concentrations [6-8]. Under China's "dual-carbon" strategy, strengthening the monitoring and evaluation of forest carbon stock dynamics is not only of ecological importance but also provides practical support for achieving carbon neutrality targets [9-11].

Karst regions are characterized by pronounced ecological fragility, shaped by the combined effects of hard and soluble carbonate rocks, well-developed fissures and caves, and monsoonal climates with synchronous heat and rainfall [12, 13]. These factors contribute to the evolution of a dual surface-subsurface hydrogeological structure, resulting in limited water storage and poor water resource availability [12, 14]. In addition, carbonate bedrock provides insufficient parent material for soil formation, leading to shallow and discontinuous soils, low resource availability, high calcium content, and weak alkalinity despite relatively fertile properties [13, 15]. Under such conditions, forest vegetation development in karst areas is constrained, with slower growth and lower overall forest coverage compared to non-karst regions [16, 17]. Although vegetation types are diverse and play essential roles in water regulation, soil conservation, and regional ecological stability [4, 18], many endemic karst plant species are highly sensitive to environmental changes and face considerable challenges in regeneration after disturbance [17, 19, 20].

In recent years, with the vigorous promotion of infrastructure development, multiple expressway projects in Guangxi have entered planning and construction phases [21]. However, as typical linear engineering works, expressways not only permanently occupy large areas of land but also involve frequent excavation, land clearing, slope modification, and drainage works, which directly damage native forests along their routes [22-24]. These construction activities typically remove large quantities of vegetation and topsoil, disrupt existing forest structures, and cause substantial declines in biomass [25, 26].

Existing studies have mainly focused on the spatial-temporal distribution of forest carbon stocks and the carbon sequestration potential of different vegetation types. For example, Lan (2019) reported that both hard and soft-broadleaf forests in Guangxi exhibit relatively high carbon stock capacities [27]. Li (2020) demonstrated that Caesalpinia sappan exhibits strong adaptability and carbon sequestration potential in the karst region of northwestern Guangxi, making it an ideal species for rocky desertification control and carbon sink enhancement [28]. Other studies by Meng (2022), Li (2024), and Zhong (2025) revealed the spatial heterogeneity of forest carbon stocks at the regional scale, highlighting the regulatory roles of topography, climate, and land use [29-31]. Nevertheless, few studies have examined the direct carbon stock losses and the compensatory effects induced by large-scale engineering projects such as expressway construction. On the other hand, research on the ecological impacts of transportation infrastructure has predominantly addressed landscape fragmentation and land-use change [32-34], while systematic quantitative evaluations of carbon sink functions remain scarce. Therefore, accurately assessing forest carbon stock reductions caused by expressway construction in karst areas, as well as the compensatory potential of subsequent greening projects, is not only of scientific significance for understanding carbon sink dynamics in karst forests but also provides practical guidance for coordinating infrastructure development with ecological conservation.

Based on the ecological fragility of karst forest ecosystems and the disturbance characteristics of expressway construction, this study aims to quantify changes in forest ecosystem carbon stocks under expressway development in karst regions. We hypothesize that expressway construction leads to measurable reductions in forest biomass and carbon stocks in areas directly affected by road building compared to undisturbed forests. Furthermore, we expect that subsequent greening and restoration measures can partially compensate for construction-induced carbon losses. Through field-based vegetation and soil surveys, biomass and carbon stock estimation, accounting of permanent land occupation–induced carbon losses, evaluation of greening project–based carbon compensation, and measurement of soil CO_2 emissions under different land-use types, this study seeks to clarify the dynamic effects of road construction and post-construction greening on forest carbon stocks and to provide quantitative support for ecological impact assessment and carbon compensation policies in expressway projects.

Materials and Methods

Study Area

The study area is located along the Du'an-Bama section of the expressway in Guangxi, southern China, which traverses the karst region over a total length of approximately 120 km. The route extends from Du'an County to Bama County in Hechi City, passing through Du'an, Dahua, and Bama counties (Fig. 1). The area lies within a subtropical monsoon climate zone, with a mean annual temperature of 19.6-21.6ºC and an average annual precipitation of about 1720 mm, characterized by warm and humid conditions with synchronous heat and

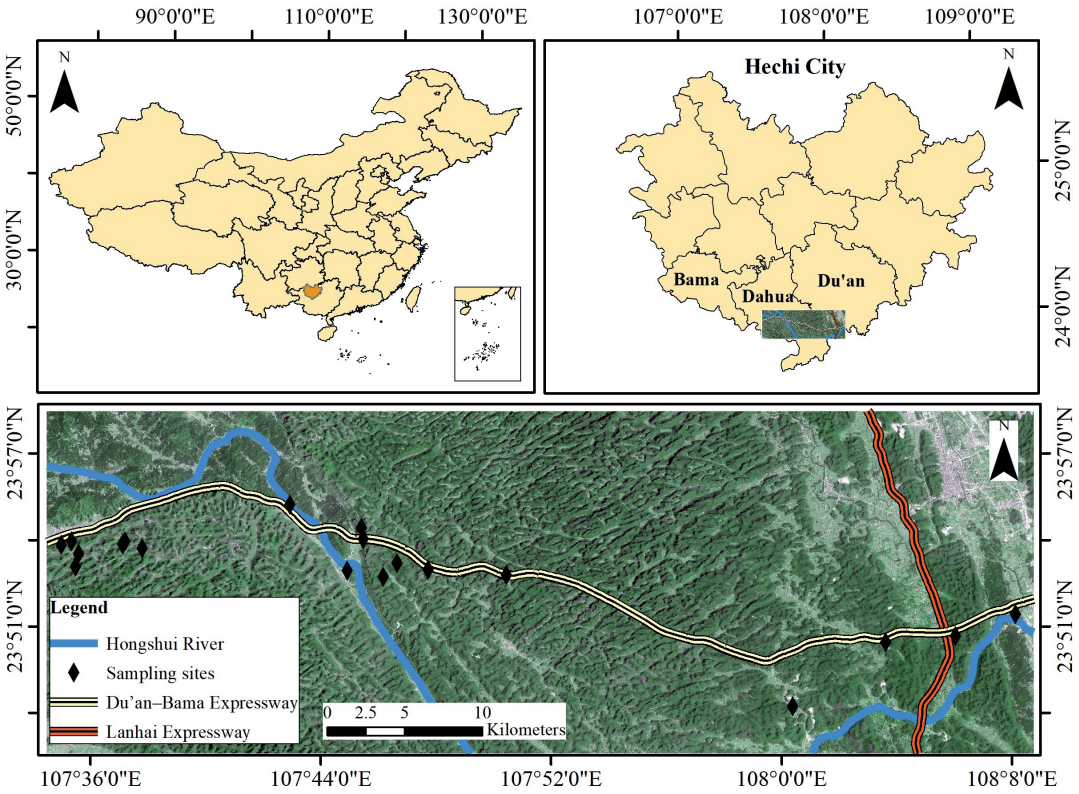

Fig. 1. Distribution of sampling plots in the study area.

rainfall [35] (China Meteorological Data Service Centre; http://data.cma.cn). Major surface water bodies include the Chengjiang River and the Hongshui River, the latter being an important tributary of the upper Xijiang River within the Pearl River system.

The study area exhibits complex geomorphological features and pronounced topographic relief, dominated by structural–erosional karst landforms such as peak-cluster depressions and valleys, with local extensions into eroded low hills [36, 37]. Carbonate rocks are widely distributed, and intense karstification provides a typical geological background of karst development [16, 38].

Soils and vegetation show distinct spatial patterns. In rocky mountain areas, soil cover averages only 10.8%, and on steep slopes with gradients greater than 45°, the coverage is merely 3.2%. Forest vegetation coverage ranges from 70% to 90%, with an average of 83%. Vegetation types are dominated by shrubs and grasslands. Natural vegetation has been highly fragmented due to long-term land use and development. Depressions and valleys are often converted into croplands, while large tracts of intact natural forests are scarce, resulting in a markedly patchy vegetation distribution.

Plot Design and Survey Methods

Plot Design

Vegetation surveys were conducted by combining literature review with field investigations, including transect surveys and typical plot surveys. The transect survey provided an overview of vegetation types, community structure, and dominant species composition within the project area. The typical plot survey further analyzed the structural characteristics of major vegetation types and key habitats. In total, 19 plots were established and geo-referenced using GPS, following the Technical Regulations for Accounting and Monitoring of Forest Land Carbon Sink (DB11/T 953-2024). The number of plots was determined to ensure representative coverage of the dominant vegetation types and disturbance conditions along the expressway corridor under complex karst terrain. Each forest plot measured 25.82 m × 25.82 m. Shrub, herb, and litter layers were investigated using quadrat methods. Within each forest plot, five 2 m × 2 m shrub quadrats were set up, and within each shrub quadrat, 1 m × 1 m subquadrats were set up for herbaceous and litter biomass surveys.

Vegetation Survey

For the tree layer, all living individuals with a diameter at breast height (DBH) greater than 5 cm were recorded, including species identity, DBH, height, and growth condition.

For the shrub layer, species composition (including trees with DBH < 2 cm), basal diameter, canopy cover, density, and height were recorded. Three average-sized standard individuals per quadrat were harvested to determine the fresh weights of stems, branches, leaves,

and roots. Subsamples of 300 g from each component (stem, branch, leaf, root) were collected for dry weight determination.

For the herbaceous layer, species composition, clump number, height, and cover were recorded. All herbaceous plants within each quadrat were harvested to measure fresh weight, and 300 g composite samples were collected for dry weight determination.

For the litter layer, thickness was measured, all litter was collected for fresh weight determination, and 200 g subsamples were taken for dry weight analysis.

Soil Survey

Soil physicochemical properties were analyzed for each vegetation plot, including soil bulk density, soil organic carbon content, soil organic carbon density, and soil organic carbon stock. Within each plot, one representative soil profile was excavated, and soil samples were collected at depth intervals of 0-10 cm, 10-20 cm, 20-40 cm, and 40-50 cm. After field sampling, soil samples collected using cutting rings were transported to the laboratory for bulk density determination. Samples were oven-dried at 105ºC to constant weight, and soil bulk density was calculated based on the oven-dried mass and the known volume of the cutting ring. Coarse fragments and visible roots were removed prior to weighing when present.

For soil organic carbon (SOC) analysis, approximately 500 g of soil was collected separately from each predefined depth interval (0-10, 10-20, 20-40, and 40-50 cm) within the same soil profile. After field sampling, soil material from the four depth intervals was combined and thoroughly homogenized to form a composite sample representing the soil profile. The homogenized composite sample was then reduced to approximately 500 g using the quartering method, sealed in plastic bags, and transported to the laboratory for further analysis. Composite samples were air-dried at room temperature, gently crushed, and passed through a 0.25 mm sieve to remove stones and plant residues. Soil organic carbon content was determined using the potassium dichromate oxidation method with external heating ($K_2Cr_2O_7$-H_2SO_4), following the standard of determination of organic matter in forest soil (LY/T1237-1999). Titration was performed using ferrous sulfate solution to quantify the amount of oxidized organic carbon.

Soil organic carbon density for each soil layer was calculated based on soil organic carbon content, soil bulk density, and layer thickness. Soil organic carbon stock at the plot level was obtained by summing the carbon densities of all soil layers within the sampled profile. These measurements were used to quantify the vertical distribution patterns of soil organic carbon and to assess differences in soil carbon stock among vegetation plots.

Soil CO_2 Emission Survey

To measure soil CO_2 emissions, soil CO_2 flux monitoring sites were preferentially established in the vicinity of vegetation plots to ensure consistency between vegetation carbon stock assessment and soil CO_2 emission measurements, following the IPCC Guidelines for National Greenhouse Gas Inventories. These sites were distributed across the major land-use types permanently occupied by the Du'an–Bama expressway, including pine forest, eucalyptus forest, *Zenia insignis* forest, bamboo forest, shrubland, grassland, and maize fields. Due to field accessibility and site-specific constraints under construction conditions, a total of 16 soil CO_2 flux sampling sites were established.

Soil CO_2 fluxes were measured using the static chamber method. To minimize diurnal variation, sampling was conducted between 09:00 and 11:00 [39]. Immediately after chamber closure, gas samples were collected using a 20 mL syringe connected to a three-way valve (first sample at 0 min, followed by additional samples at 10 min intervals, for a total of four samples over 30 min). Gas samples were stored in headspace vials and analyzed at the Guangxi Key Laboratory of Karst Dynamics, Ministry of Natural Resources, using an Agilent SP1 7890-0468 gas chromatograph (CO_2 detection range: 0-5000 ppm, precision: 0.01 ppm). Ambient air temperature and pressure were recorded simultaneously.

Vegetation Survey of Greening Projects

In this study, greening projects refer specifically to vegetation restoration measures planned within the permanent land occupation boundary of the Du'an–Bama expressway. These measures are spatially confined to engineering units directly associated with expressway construction, including green belts along the road, embankment and excavation slopes, interchanges, tunnel entrances, service areas, and toll stations. All greening areas considered in this assessment are located within the expressway right-of-way and do not include off-site or independent ecological compensation projects.

Considering the specific characteristics of afforestation associated with expressway green belts, interchanges, and toll stations, the greening projects adopted a mixed structure of forest, shrubland, and grassland. As the Du'an–Bama section was still under construction and greening had not yet been implemented at the time of investigation, field plot surveys could not be conducted. Instead, officially approved greening design plans were collected, which serve as mandatory implementation specifications during the construction stage and include detailed information on planting area, tree species, number of individuals, DBH, height, and crown width; shrub cultivation methods, species composition, number, height, and crown width; and herb species, coverage area, and height. These standardized

engineering parameters were used as inputs for biomass estimation through established allometric equations, thereby converting greening design information into quantitative estimates of biomass and carbon stocks.

Biomass and Carbon Stock Estimation Methods and Parameter Settings

Tree Layer Biomass Estimation

Tree layer biomass was divided into aboveground and belowground components. For aboveground tree biomass, in the absence of species-specific allometric equations, this study adopted the generalized allometric model proposed by Chave (2014) [40], which was developed from global tropical forest plot data. Belowground biomass was estimated using the root-to-shoot ratio default values recommended by the IPCC. The biomass of the tree layer was calculated as follows:

$$W_{tree,above} = 10^{-3} \times \exp\left[-1.803 - 0.976E + 0.976\ln(\rho) + 2.673\ln(D) - 0.0299(D)^2\right] \quad (1)$$

$$W_{tree,sum} = \frac{\sum_{i=1}^{n} W_{tree,above} \times (1+R)}{S_{tree,plot}} \quad (2)$$

In the equations, $W_{tree,above}$ represents the aboveground biomass of an individual tree (kg); D is the diameter at breast height (cm); ρ denotes wood density (g/cm³); E is the environmental stress factor; R refers to the root-to-shoot ratio of trees in the tree layer; n is the total number of trees within the plot; $W_{tree,sum}$ represents the tree layer biomass per unit area of the plot (kg/m²; 1 kg/m² = 10 t/hm²); and $S_{tree,plot}$ is the plot area of the tree layer (m²).

Shrub Layer Biomass Estimation

Shrub biomass was estimated based on the number of shrubs/clumps, the fresh weights of sampled individuals, and the average fresh weight of standard shrubs, using the following equations:

$$m_{shrub} = P_{shrub} \times \frac{\sum_{i}^{n} M_{standard,wet}}{n_{standard}} \quad (3)$$

$$M_{shrub} = K \times m_{shrub} \times 10^{-3} \quad (4)$$

$$M_{shrub,sum} = \frac{\sum_{i}^{n} M_{shrub}}{N_{plot} \times S_{shrub,plot}} \quad (5)$$

Where m_{shrub} is the average dry biomass per standard shrub (g); P_{shrub} is the dry-to-fresh weight ratio; $M_{standard,wet}$ is the average fresh weight of standard shrubs (g); $n_{standard}$ is the number of standard shrubs; M_{shrub} is the total dry biomass of shrubs per quadrat (kg); K is the total number of shrubs in the quadrat; $M_{shrub,sum}$ is the shrub layer biomass per unit area (kg/m²; 1 kg/m² = 10 t/hm²); N_{plot} is the number of quadrats; and $S_{shrub,plot}$ is the quadrat area (m²).

Herbaceous Layer Biomass Estimation

Herbaceous layer biomass was calculated from the fresh and dry weights of samples collected in quadrats:

$$M_{herb} = \frac{M_{herb,wet} \times P_{herb}}{S_{herb,plot}} \quad (6)$$

Where M_{herb} is the herbaceous layer biomass per unit area (kg/m²; 1 kg/m² = 10 t/hm²); $M_{herb,wet}$ is the total dry weight of herbs in a quadrat (kg); P_{herb} is the dry-to-fresh weight ratio; and $S_{herb,plot}$ is the quadrat area (m²).

Litter Layer Biomass Estimation

Litter biomass was estimated similarly, based on fresh and dry weights:

$$M_{litter} = \frac{M_{litter,wet} \times P_{litter}}{S_{litter,plot}} \quad (7)$$

Where M_{litter} is the litter biomass per unit area (kg/m²; 1 kg/m² = 10 t/hm²); $M_{litter,wet}$ is the total dry weight of litter in a quadrat (kg); P_{litter} is the dry-to-fresh weight ratio; and $S_{litter,plot}$ is the quadrat area (m²).

Vegetation Carbon Stock Estimation

The total carbon stock of vegetation was calculated as the sum of carbon pools in all vegetation layers. For each vegetation type, carbon stock was derived from the product of biomass and carbon content. Carbon content coefficients were obtained from the Technical regulations for accounting and monitoring of forest land carbon sink [41] and Fang (1996) [42].

Soil Organic Carbon Stock Estimation

Soil carbon stock was estimated using a layer-by-layer accumulation approach. The average soil organic carbon density of each soil layer was calculated based on soil bulk density, organic carbon content, and soil thickness, and subsequently integrated over the corresponding land-use or forest type area. The calculation followed the framework of the Technical Specification for Forest Ecosystem Carbon Stock Measurement (LY/T 3330-2022) with appropriate simplification. The soil organic carbon density per unit area was calculated as follows:

$$T_j = \sum_{i=1}^{k} \rho_i \times C_i \times H_i \quad (8)$$

Where T_j is the average soil organic carbon density of the j-th land-use or forest type (g·cm^{-2}); ρ_j is the soil bulk density of the i-th soil layer (g·cm^{-3}); C_i is the soil

organic carbon content of the i-th layer (%); H_i is the thickness of the i-th soil layer (cm); k is the number of soil layers.

Based on the soil organic carbon density, the total soil organic carbon stock of the study area was calculated as:

$$M_d = \sum_{j=1}^{n} A_j \times T_j \quad (9)$$

Where M_d is the total soil organic carbon stock of the study area (tC); A_j is the area of the j-th land-use or forest type (hm²); T_j is the corresponding soil organic carbon density per unit area.

Soil CO_2 Flux Estimation

Soil CO_2 emission rates were calculated from CO_2 concentration data collected by the static chamber method, combined with chamber pressure and temperature, as follows [43]:

$$F = \frac{M}{V_0} \times \frac{P}{P_0} \times \frac{T_0}{T} \times H \times \frac{dc}{dt} \quad (10)$$

Where F is the soil respiration rate; M is the molar mass of CO_2; P_0 and T_0 are the standard pressure and temperature of air; V_0 is the molar volume of CO_2 under standard conditions; H is the effective chamber height; P and T are the actual chamber pressure and temperature during sampling; and dc/dt is the slope of the regression line of CO_2 concentration change over time.

Carbon Stock of Greening Projects

The total carbon stock of greening projects was calculated as the sum of above- and belowground biomass carbon pools of forest, shrubland, and grassland. For forest, aboveground biomass was estimated from DBH and height using species-specific equations.

Evergreen broadleaf species:

Stem: $W = 0.000023324\ (D^2H)^{0.9750}$;

Branches: $W = 0.000021428\ (D^2H)^{0.906}$;

Leaves: $W = 0.00001936\ (D^2H)^{0.6779}$

Masson pine (*Pinus massoniana*) and other conifers:

Stem: $W = 0.00004726\ (D^2H)^{0.8865}$;

Branches: $W = 0.000001883\ (D^2H)^{1.0677}$;

Leaves: $W = 0.000000459\ (D^2H)^{1.0968}$

Where W is biomass (t); D is DBH (cm); and H is tree height (m).

Belowground biomass was estimated as:

Evergreen broadleaf species: Broot = Babove × 0.164

Masson pine and other conifers: Broot = Babove × 0.160

For understory vegetation:

$Yc = 0.34604\ (CH)^{0.93697}$; $Yg = 0.32899\ (CH)^{0.9068}$

Where Yc and Yg are the biomass of shrubs and herbs per unit area (t/hm²); H is plant height (m); and C is canopy cover (%).

Results and Discussion

Soil Carbon Stock

Soil survey results indicated pronounced heterogeneity in soil organic carbon (SOC) storage across the study area, which was closely associated with variations in soil thickness, bulk density, and organic carbon content [13]. In the typical karst setting of the study area, soils are characteristically shallow, discontinuous, and highly heterogeneous due to strong lithological and geomorphic constraints [12]. Soils developed on mountain slopes at the margins of peak-cluster depressions and valleys were generally shallow, with thicknesses mostly ranging from 5 to 10 cm and only a few profiles reaching up to 20 cm. In contrast, soils in valley bottoms, depressions, and plains exhibited substantially greater thickness, locally reaching up to 50 cm, thereby providing a larger capacity for SOC accumulation [44].

Vegetation type further modulated SOC storage patterns by influencing soil development and physical properties. Forested plots were generally associated with deeper soils, often approaching 40 cm, which favored higher SOC stocks. In contrast, soils under shrublands, shrub-grass mixtures, and grasslands were predominantly shallow (5-10 cm), constraining their overall carbon storage potential. Soil bulk density (Fig. 2a)), as a key factor regulating SOC storage, was generally high across the study area, with most plots ranging from 1.0 to 1.5 $g \cdot cm^{-3}$, indicating relatively poor structural porosity and limited water- and nutrient-retention capacity [45]. A few plots, such as DB002 and DB014, exhibited lower bulk density values (<0.75 $g \cdot cm^{-3}$), which may facilitate greater SOC preservation by improving soil structure and reducing organic matter mineralization. SOC content (Fig. 2b)) showed relatively moderate variability among plots, with most values falling within the range of 1.0-2.5%. Higher SOC contents (approximately 3.5%) were observed in plots DB002 and DB014. The coexistence of relatively high SOC content and low bulk density in these plots suggests favorable conditions for organic matter accumulation and stabilization. However, when SOC content was integrated with soil bulk density and profile thickness, SOC density (Fig. 2c)) exhibited less pronounced variation among vegetation types, generally ranging between 15 and 20 $mgC \cdot cm^{-3}$. Vertical profiles consistently showed a gradual decline in SOC density with increasing soil depth, reflecting surface-dominated organic carbon inputs.

Overall, the spatial pattern of SOC storage in the study area was primarily controlled by the combined effects of soil thickness, bulk density, and SOC content (Fig. 2). Forested plots with deeper soils and more favorable physical properties exhibited higher SOC storage capacity, whereas shallow soils under shrubland and grassland constrained carbon accumulation despite comparable SOC contents. These results highlight the

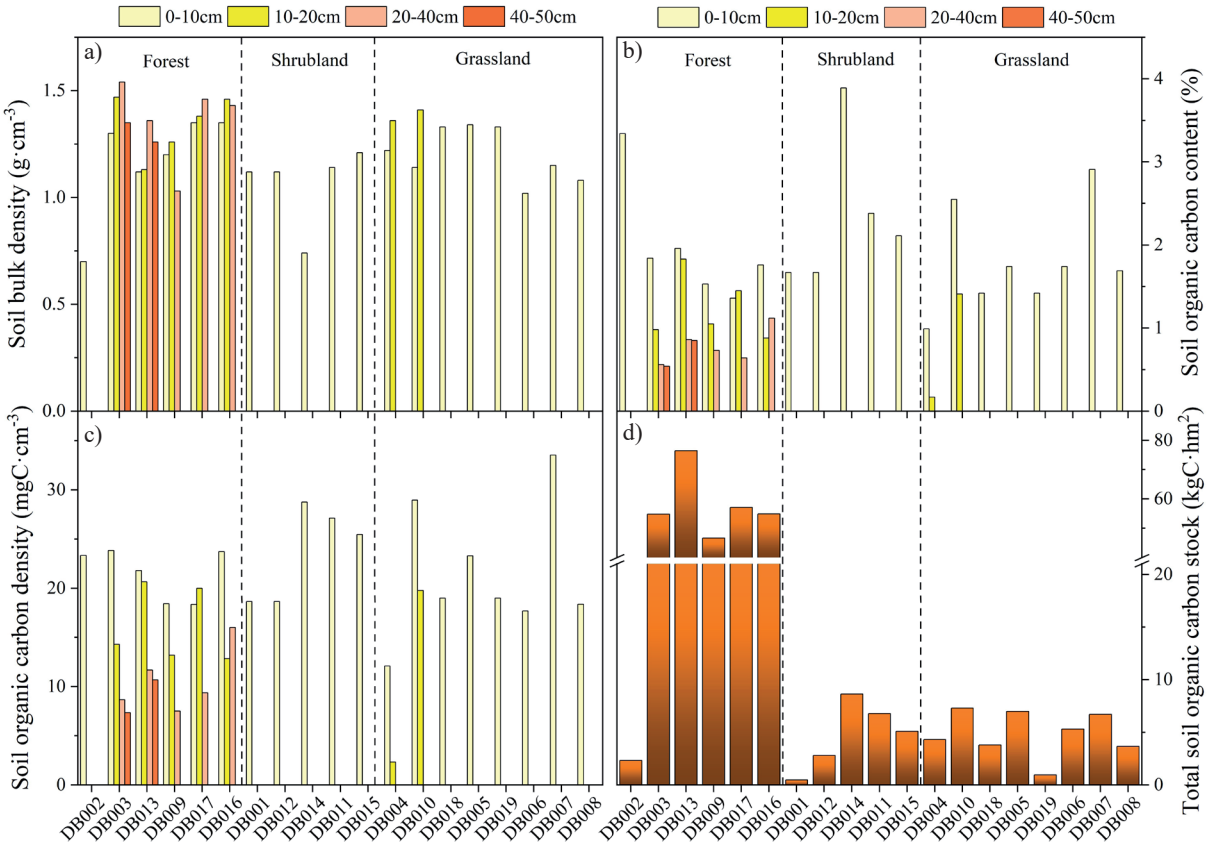

Fig. 2. Soil properties controlling soil organic carbon (SOC) storage across different vegetation plots: a) soil bulk density; b) SOC content; c) SOC density; d) total SOC stock.

dominant role of soil physical constraints in regulating SOC storage in karst ecosystems.

Biomass and Carbon Stock Characteristics of Different Vegetation Types

This section aims to quantify the biomass and carbon stock characteristics of representative vegetation types along the Du'an–Bama expressway corridor, providing essential unit-area carbon density parameters for estimating carbon losses associated with permanent land occupation due to highway construction. Rather than serving as a purely ecological comparison, the analysis of different vegetation types is designed to establish baseline carbon stock values corresponding to land-use categories affected by expressway development.

Biomass and carbon stock were calculated for different community types across plots, and their distribution among vegetation layers was statistically analyzed (Table 1). Overall, forest plots exhibited higher biomass than shrublands and grasslands. Among them, the *Pinus massoniana* community had the highest biomass, approximately three times greater than the national average value of 81.14 t·hm^{-2} for *Pinus massoniana* forests reported by Fang (1996) [42]. This marked difference is likely due to the higher planting density of *Pinus massoniana* in the plots and the favorable subtropical climate with sufficient heat, moisture, and light that promotes growth. In contrast, the *Cyclobalanopsis glauca* and *Bambusa textilis* communities exhibited relatively low biomass, comparable to some shrubland plots. Specifically, the biomass of *Cyclobalanopsis glauca* communities was about eight times lower than the national average value of 163.67 t·hm^{-2} [42]. Such reductions can be attributed to the shallow soils, high bulk density, and high rock exposure characteristic of karst regions, which severely limit vegetation growth.

Within shrubland types, the total biomass among different communities showed little variation, though the *Pterolobium punctatum* community had the highest shrub biomass, exceeding that of *Cyclobalanopsis glauca* and *Zenia insignis* communities by more than tenfold. Grassland plots generally exhibited lower overall biomass; however, the two *Miscanthus floridulus* plots displayed notably high herbaceous biomass, reaching 21.93 t·hm^{-2} and 25.74 t·hm^{-2}, far exceeding herbaceous biomass levels recorded in forest and shrubland plots.

The distribution of carbon stocks followed the same general pattern as biomass (forest > shrubland > grassland), reflecting the stronger carbon stock capacity of highly lignified vegetation. The *Pinus massoniana* community had the highest carbon stock at 116.08 tC·hm^{-2}, representing the strongest carbon sequestration capacity in the study area. In contrast, the *Cyclobalanopsis glauca* community exhibited

only 8.76 tC·hm^{-2}, lower even than shrubland types lacking tree layers, such as the *Clerodendrum-Millettia* community, reflecting poor carbon stock capacity. In addition, the *Miscanthus* plots had markedly higher carbon stocks than other herbaceous communities, suggesting that under adequate light and high vegetation cover, *Miscanthus* grasslands can accumulate a significant amount of carbon stock.

Integration with soil survey results further revealed that spatial differences in biomass and carbon stocks were partly consistent with soil thickness and organic matter content. Dominant tree species such as *Pinus massoniana* tended to occur in forest plots with deeper soils and moderate bulk density, where favorable physicochemical conditions supported biomass and carbon stock accumulation. Conversely, *Cyclobalanopsis glauca*, shrubland, and some grassland communities were mostly distributed in areas with shallow soils and limited organic matter, thereby exhibiting lower carbon stock capacity.

In summary, the observed differences in biomass and carbon stock among vegetation community types not only highlight the spatial characteristics of carbon stock capacity in karst forest ecosystems but also provide a basis for further analysis of the impacts of expressway construction on forest ecosystem carbon sink functions.

Carbon Loss from Permanent Land Occupation by Expressway Construction

According to survey data provided by the construction unit of the Du'an–Bama expressway project (including the total area of permanent land occupation and the occupied area of each vegetation type), the total permanent land occupation in the study area was approximately 217.22 hm². The occupied areas of representative vegetation types were as follows: maize 106.57 hm², *Zenia insignis* 2.00 hm², *Cyclobalanopsis glauca* 3.50 hm², bamboo 0.69 hm², *Eucalyptus urophylla* 65.54 hm², *Pinus massoniana* 1.50 hm², *Vitex negundo* 10.58 hm², and *Miscanthus floridulus* 26.84 hm². Based on the unit-area biomass and carbon stock values obtained from vegetation surveys (Table 1), the total biomass and carbon losses resulting from expressway construction were calculated as the sum of the products of these values and the corresponding occupied areas (Table 2).

When calculating the carbon loss from permanent land occupation, it was noted that shrubland and grassland vegetation types exhibited complex intergrowth and species combinations, making precise estimation based on a single species impractical. Therefore, average unit-area biomass and carbon stock values from shrubland and grassland plots in the vegetation survey were used as representative parameters, providing a more reasonable reflection of the overall carbon loss characteristics of these communities.

Furthermore, since soils from occupied land were reused and placed in spoil disposal sites for vegetation restoration, and thus remained within the study region, soil carbon stocks were assumed to remain largely unchanged. Consequently, only vegetation carbon losses were included in the calculation. Final estimates indicated that permanent land occupation by the Du'an–Bama expressway project resulted in a total biomass loss of 10207.21 t, derived from the permanently occupied area and unit-area vegetation biomass, corresponding to a carbon loss of 4601.89 tC (Table 2).

For comparison, Hao (2021) [47] reported that permanent land occupation associated with the Gongyu expressway in the Sanjiangyuan region (1587 hm²) led to a vegetation biomass loss of 3336.7 t, equivalent to a unit-area biomass loss of 2.10 t·hm^{-2}. In contrast, the Du'an–Bama expressway produced a unit-area biomass loss of 46.99 t·hm^{-2}, which is 22.37 times greater, indicating that the destructive impact of expressway construction on forest vegetation biomass is far more severe in karst regions than in non-karst areas.

This disparity can be largely attributed to the unique ecological and environmental characteristics of karst regions. On the one hand, hydrological and climatic conditions in karst areas are more favorable for vegetation growth, leading to higher biomass and carbon stock per unit area in forest communities. On the other hand, the shallow soil development and slow vegetation regeneration rates in karst ecosystems greatly limit natural recovery. As a result, ecological damage caused by human activities cannot be readily compensated through natural succession over long timescales. Therefore, the implementation of greening projects can partially compensate for the biomass and carbon stock losses caused by permanent land occupation, enhance the stability and resilience of regional ecosystems, and play an essential role in ecological restoration.

Estimation of Biomass and Carbon Stock Compensation by Greening Projects

The study area is situated in a subtropical humid monsoon climate zone, with favorable hydrothermal conditions and a stable natural environment conducive to vegetation growth. Although expressway construction inevitably occupies a certain amount of land, greening projects are typically implemented within permanently occupied areas, such as slopes, central medians, tunnel entrances, and service areas. In addition, temporary land occupation can also achieve partial ecological compensation through post-construction revegetation.

To evaluate the compensatory effects of engineering restoration on biomass and carbon stock losses, greening project design and planning documents of the Du'an–Bama expressway were analyzed to calculate the areas of central medians, tunnel entrances, slopes, interchanges, and service areas designated for afforestation. Based on greening plans, shrub cover was estimated at 27.55% with an average height of 1.00 m, and grassland cover at 97.83% with an average height

Table 1. Comparison of biomass and carbon storage among different vegetation types.

	Plot No.	Typical plot	Tree layer		Shrub layer		Herb layer		Litter layer		Total	
			Biomass	Carbon storage	Biomass	Carbon storage	Biomass	Carbon storage	Biomass	Carbon storage	Biomass	Carbon storage
Forest	DB002	*Cyclobalanopsis glauca*	13.64	6.54	1.08	0.50	0.23	0.08	3.35	1.64	18.30	8.76
	DB003	*Zenia insignis*	80.45	38.58	2.84	1.33	2.94	0.96	5.51	2.70	91.74	43.57
	DB013	*Pinus massoniana*	229.56	113.93	—	—	0.14	0.05	4.29	2.10	233.99	116.08
	DB009	*Eucalyptus urophylla*	63.62	29.90	—	—	3.55	1.16	2.73	1.34	69.90	32.40
	DB017	*Eucalyptus urophylla*	165.29	77.69	—	—	5.32	1.74	5.00	2.45	175.61	81.88
	DB016	*Bambusa textilis*	18.90	8.89	—	—	0.93	0.30	3.62	1.77	23.45	10.97
Shrubland	DB001	*Pterolobium punctatum*	—	—	14.34	6.70	2.18	0.72	2.07	1.01	18.59	8.43
	DB012	*Pterolobium punctatum*	—	—	22.26	10.40	1.56	0.51	4.43	2.17	28.25	13.09
	DB014	*Phanera championii*	—	—	17.15	8.01	1.27	0.42	4.44	2.18	22.86	10.61
	DB011	*Vitex negundo*	—	—	10.44	4.88	1.93	0.64	0.85	0.42	13.22	5.93
	DB015	*Vitex negundo*	—	—	8.40	3.92	0.12	0.04	1.3	0.64	9.82	4.60
Grassland	DB004	*Miscanthus floridulus*	—	—	—	—	21.93	7.24	2.35	1.15	24.28	8.39
	DB010	*Miscanthus floridulus*	—	—	—	—	25.74	8.49	3.47	1.70	29.21	10.19
	DB018	*Imperata cylindrica*	—	—	—	—	14.08	4.65	2.22	1.09	16.30	5.74
	DB005	*Arundinella hirta*	—	—	—	—	7.05	2.33	1.95	0.96	9.00	3.28
	DB019	*Arundinella hirta*	—	—	—	—	8.28	2.73	2.14	1.05	10.42	3.78
	DB006	*Dicranopteris dichotoma*	—	—	—	—	9.40	3.10	3.86	1.89	13.26	4.99
	DB007	*Dicranopteris dichotoma*	—	—	—	—	7.35	2.43	2.26	1.11	9.61	3.53
	DB008	*Dicranopteris dichotoma*	—	—	—	—	3.34	1.10	5.38	2.64	8.72	3.74

Note: Biomass and carbon stock in this table are expressed on a unit-area basis ($t \cdot hm^{-2}$ and $t\ C \cdot hm^{-2}$, respectively), and "—" indicates no data.

Table 2. Summary of carbon stock loss from permanent land occupation of the project.

Vegetation type	Representative species	Biomass per unit area ($t \cdot hm^{-2}$)	Carbon stock per unit area ($tC \cdot hm^{-2}$)	Project occupation area (hm^2)	Biomass loss (t)	Carbon loss (tC)
Dryland	*Zea mays* [46]	8.87	3.01	106.57	945.28	320.78
Forest	*Zenia insignis*	91.74	43.57	2.00	183.48	87.14
	Cyclobalanopsis delavayi	18.3	8.76	3.50	64.05	30.66
	Bamboo forest	23.45	10.97	0.69	16.18	7.57
	Eucalyptus urophylla	122.76	57.14	65.54	8045.69	3744.96
	Pinus massoniana	233.99	116.08	1.50	350.99	174.12
Shrubland	*Vitex negundo*	18.55	8.53	10.58	196.26	90.25
Grassland	*Miscanthus floridulus*	15.10	5.46	26.84	405.28	146.41
Total				217.22	10207.21	4601.89

of 0.1 m. For forest, biomass was estimated from DBH, height, and number of individuals using allometric equations. The average biomass values of shrubs, grasses, and forests were calculated as 6.65, 2.93, and 4.45 $t \cdot hm^{-2}$, respectively, with a combined total of 14.03 $t \cdot hm^{-2}$ (Table 3). Subsequently, the biomass of different greening components was obtained by multiplying unit-area biomass by the corresponding greening area, and carbon stocks were derived based on the mean carbon content of each vegetation type (Table 4).

Table 3. Biomass of different vegetation types restored by greening projects.

Vegetation type	Total area (m^2)	Canopy cover (%)	Mean height (m)	Biomass ($t \cdot hm^{-2}$)
Shrubland	195093	27.55	1.00	6.65
Grassland	692853	97.83	0.10	2.93
Forest				4.45
Total				14.03
Aboveground biomass of forest: 3.82 $t \cdot hm^{-2}$; belowground biomass: 0.63 $t \cdot hm^{-2}$.				

Table 4. Biomass and carbon stock restored by greening projects.

Greening project	Greening area (hm^2)	Biomass (t)				Carbon stock (tC)			
		Forest	Shrubland	Grassland	Total	Forest	Shrubland	Grassland	Total
Central median	4.70	20.89	31.30	13.79	65.98	10.22	14.62	4.51	29.35
Tunnel entrance	30.17	133.94	200.72	88.45	423.11	65.54	93.77	28.92	188.23
Embankment slope	1.29	5.74	8.61	3.79	18.15	2.81	4.02	1.24	8.07
Excavation slope	0.21	0.92	1.38	0.61	2.90	0.45	0.64	0.20	1.29
Branch connection line	0.12	0.55	0.82	0.36	1.73	0.27	0.38	0.12	0.77
Interchange	10.88	48.30	72.37	31.89	152.57	23.63	33.81	10.43	67.87
Service areas and toll stations	23.45	104.10	156.00	68.75	328.86	50.94	72.89	22.48	146.31
Total	70.82	314.44	471.20	207.65	993.30	153.86	220.15	67.90	441.90

Note: The carbon contents of Forest, Shrubland, and Grassland were set at 0.4893, 0.4672, and 0.3270, respectively [27]. Carbon stock values in this table represent total restored carbon stocks (tC), calculated by multiplying unit-area biomass by the corresponding greening area.

A key limitation of this study is that field-based biomass surveys for greening areas were not feasible because the expressway was still under construction during the study period. Consequently, carbon stock estimates for greening projects were derived from approved engineering design documents, including planned vegetation types, planting densities, coverage, and structural parameters. Although actual post-construction vegetation establishment and early growth may deviate from design assumptions, such deviations mainly reflect variability in growth performance and establishment success, rather than uncertainty in vegetation type, spatial extent, or the initial structural parameters defined by the approved greening design. In this context, these design documents, developed through standardized engineering procedures and serving as mandatory implementation guidelines, provide a consistent and well-defined basis for construction-stage carbon stock estimation.

Results indicated that the permanent land occupation of the Du'an–Bama expressway caused a biomass loss of 10207.21 t (Table 2), of which only 993.30 t was compensated by greening projects, resulting in a net loss of approximately 9213.91 t and a biomass recovery rate of 9.73%. Similarly, the carbon stock loss was 4601.89 tC, with 441.90 tC compensated, leaving an actual loss of 4159.99 tC and a recovery rate of 9.60%. These findings suggest that even when greening projects achieve their design targets, their overall compensation for carbon stock losses remains limited.

This insufficient compensation is mainly attributable to the vegetation composition and growth stage of the greening projects. Vegetation in greening areas was dominated by shrubs and herbaceous species, which accumulate relatively low biomass during the early stages of establishment. Forest species were limited in number and characterized by small DBH and height, with carbon sequestration potential not yet fully realized. In addition, shallow soils and high bedrock exposure typical of karst regions further constrain vegetation growth rates, thereby contributing to the low recovery efficiency. Notably, however, the ecological compensation effect of greening projects is long-term. As vegetation continues to grow, biomass and carbon stocks are expected to increase annually, gradually narrowing the gap caused by initial losses.

Evaluation of Forest Carbon Sink/Source under Expressway Construction

The greening measures implemented along the expressway adopted a mixed structure of forests, shrubs, and grasses, dominated by shrubs. Thus, the restored vegetation can be regarded as open forest or shrubland. According to the function describing the relationship between productivity (y) and biomass (x) for open forests or shrublands proposed by Fang (1996) [42]: $1/y = 1.27/x^{1.196} + 0.056$. x represents the total unit-area biomass of the three vegetation types in the greening project (Table 3). Based on this relationship, the productivity (y) was calculated as 9.10 $t \cdot hm^{-2} \cdot a^{-1}$. Accordingly, the greening project restored 644.16 $t \cdot a^{-1}$ of biomass, suggesting that it would take approximately 14.4 years to fully compensate for the permanent land occupation loss of 9213.91 t of biomass.

In addition, permanent land occupation involved fully paved surfaces without vegetation cover, where underlying soils were sealed and were unable to release CO_2 to the atmosphere [48]. This reduction in emissions was considered an additional carbon retention effect [49]. Soil CO_2 emission monitoring results showed fluxes of 6.11, 12.37, 9.14, 10.96, 13.95, 3.19, and 8.98 $tC \cdot hm^{-2} \cdot a^{-1}$ for pine forest, eucalyptus forest, *Zenia insignis*, bamboo, shrubland, grassland, and maize fields, respectively. The mean emission rate across these land-use types was 9.24 $tC \cdot hm^{-2} \cdot a^{-1}$. With a hardened surface area of 146.4 hm^2 (total permanent land occupation minus greening area), the annual reduction in soil CO_2 emissions was equivalent to 1352.74 tC. It should be noted that soil CO_2 fluxes in this study were measured during the stable period of vegetation growth, when soil biological activity is relatively active and less variable. This monitoring period is therefore considered broadly representative of annual soil respiration conditions [39]. However, soil CO_2 emissions are influenced by multiple environmental factors, and seasonal variability may affect flux magnitudes. As a result, the annual soil CO_2 emissions estimated in this study should be regarded as approximations rather than exact values, which represents a limitation of the present work.

For the greening area, vegetation productivity was 9.10 $t \cdot hm^{-2} \cdot a^{-1}$. With an average carbon content of 0.43, this corresponded to a carbon stock productivity of 3.91 $tC \cdot hm^{-2} \cdot a^{-1}$. Over the 70.82 hm^2 of greening area, this amounted to an additional 276.91 $tC \cdot a^{-1}$. The combined contributions of vegetation carbon sequestration from greening projects and carbon retention from paved surfaces yielded a total of 1629.65 $tC \cdot a^{-1}$. Based on this value, the carbon loss of 4601.89 tC caused by permanent land occupation could be fully compensated within only 2.6 years, approximately 5.6 times faster than relying on greening projects alone.

The estimated 2.6 years compensation cycle has important policy implications for carbon management in expressway construction projects, particularly in karst regions. This result suggests that when both greening measures and the suppression of soil CO_2 emissions by hardened surfaces are incorporated into carbon accounting, the net carbon balance of infrastructure projects may recover much faster than indicated by vegetation restoration alone. From a policy perspective, this highlights the importance of adopting an integrated carbon accounting framework that considers both biological carbon sequestration and engineering-induced changes in soil carbon fluxes. Such an approach can support more realistic evaluations of project-level carbon neutrality pathways, inform the design of

expressway greening standards, and provide quantitative evidence for incorporating transportation infrastructure into regional carbon management and compensation schemes.

Conclusions

This study demonstrated that biomass and carbon stock varied significantly among vegetation types, with forests exhibiting markedly higher carbon stock capacity than shrublands and grasslands. The *Pinus massoniana* community had the highest carbon stock, while the *Miscanthus floridulus* community showed relatively strong carbon sequestration potential among grassland types. Soil physicochemical properties, particularly soil thickness, bulk density, and SOC content, were also found to strongly constrain carbon stock capacity across vegetation types.

The construction of the Du'an-Bama expressway permanently occupied 217.22 hm^2 of land in the karst region, resulting in a biomass loss of 10207.21 t and a carbon stock loss of 4601.89 tC. Greening projects implemented within the project area were estimated to compensate for 993.30 t of biomass and 441.90 tC of carbon, corresponding to recovery rates of 9.73% and 9.60%, respectively. When accounting for the annual carbon sequestration productivity of restored vegetation and the carbon retention effect of sealed soils beneath hardened road surfaces, the system was estimated to achieve an annual net carbon gain of 1629.65 tC, suggesting that the total carbon loss from permanent land occupation could be offset within approximately 2.6 years under the accounting framework of this study.

Overall, expressway construction caused substantial disturbance to the carbon sink function of forest ecosystems. Permanent land occupation led to significant reductions in carbon stock capacity, while subsequent greening projects and the carbon retention effect of hardened road surfaces contributed to gradual recovery. Reducing carbon losses from permanent land occupation, shortening recovery times, and improving restoration efficiency should be prioritized in future expressway design and ecological management practices.

Acknowledgments

This research was supported by the National Natural Science Foundation of China [Grant Number 42361144885]; the Natural Science Foundation of Guangxi [Grant Numbers GuikeAB25069159, GuikeAB24010154]; the Project of the China Geological Survey [Grant Number DD20230547]; and the Natural Resources Science and Technology Strategic Research Project [Grant Number 2023-ZL-23].

Conflict of Interest

The authors declare no conflict of interest.

References

1. FRIEDLINGSTEIN P., O'SULLIVAN M., JONES M.W., ANDREW R.M., BAKKER D.C.E., HAUCK J. Global Carbon Budget 2023. Earth System Science Data, **15** (12), 5301, **2023**.
2. SCHIERMEIER Q. Increased flood risk linked to global warming. Nature, **470**, **2011**.
3. WANG P.Y., HUI P.H., XUE D.K., TANG J.P. Future projection of heat waves over China under global warming within the CORDEX-EA-II project. Climate Dynamics, **53** (1-2), 957, **2019**.
4. LIU C.C., WANG B., GUO K., LI X.K., HOU M.F., LIU Y.G. Karst vegetation classification system of China. Guihaia, **41** (10), 1618, **2021** [In Chinese].
5. PENG B., ZHOU Z.Y., CAI W.X., LI M.X., XU L., HE N.P. Maximum potential of vegetation carbon sink in Chinese forests. Science of the Total Environment, **905**, 167325, **2023**.
6. ZHAO X., MA X.W., CHEN B.Y., SHANG Y.P., SONG M.L. Challenges toward carbon neutrality in China: Strategies and countermeasures. Resources Conservation and Recycling, **176**, 105959, **2022**.
7. KEENAN T.F., PRENTICE I.C., CANADELL J.G., WILLIAMS C.A., WANG H., RAUPACH M., COLLATZ G.J. Recent pause in the growth rate of atmospheric CO_2 due to enhanced terrestrial carbon uptake. Nature Communications, **7** (1), 13428, **2016**.
8. ZHANG L., REN X.L., WANG J.B., HE H.L., WANG S.Q., WANG M.M., PIAO S.L., YAN H., JU W.M., GU F.X., ZHOU L., NIU Z.E., GE R., LI Y.Y., LV Y., YAN H.M., HUANG M., YU G.R. Interannual variability of terrestrial net ecosystem productivity over China: regional contributions and climate attribution. Environmental Research Letters, **14** (1), **2019**.
9. PIAO S.L., YUE C., DING J.Z., GUO Z.T. Perspectives on the role of terrestrial ecosystems in the 'carbon neutrality' strategy. Science China-Earth Sciences, **65**, (6), 1178, **2022**.
10. WANG J., FENG L., PALMER P.I., LIU Y., FANG S.X., BOSCH H., O'DELL C.W., TANG X.P., YANG D.X., LIU L.X., XIA C.Z. Large Chinese land carbon sink estimated from atmospheric carbon dioxide data. Nature, **586** (7831), 720, **2020**.
11. HE H., WANG S., ZHANG L., WANG J., REN X., ZHOU L., PIAO S., YAN H., JU W., GU F., YU S., YANG Y., WANG M., NIU Z., GE R., YAN H., HUANG M., ZHOU G., BAI Y., XIE Z., TANG Z., WU B., ZHANG L., HE N., WANG Q., YU G. Altered trends in carbon uptake in China's terrestrial ecosystems under the enhanced summer monsoon and warming hiatus. National Science Review, **6** (3), 505, **2019**.
12. YUAN D.X. Karst Science in China. Geological Publishing House, Beijing, China, **1994** [In Chinese].
13. CAO J.H., YUAN D.X., ZHANG C., JIANG Z.C. Karst Ecosystem Constrained by Geological Conditions in Southwest China. Earth and Environment, (1), 1, **2004** [In Chinese].
14. HUANG F., CAO J.H., ZHU T.B., FAN M.Z., REN M.M. CO_2 Transfer Characteristics of Calcareous Humid

Subtropical Forest Soils and Associated Contributions to Carbon Source and Sink in Guilin, Southwest China. Forests, **11** (2), **2020**.
15. JIANG Z.C., YUAN D.X., CAO J.H., QIN X.Q., HE S.Y., ZHANG C. A Study of Carbon Sink Capacity of Karst Processes in China. Acta Geoscientica Sinica, **33** (2), 129, **2012** [In Chinese].
16. ZHANG S., ZHANG Y., XIONG K., YU Y., HE C., ZHANG S., WANG Z. Construction of forest ecological security patterns based on MSPA model and circuit theory in the Desertification Control forests in South China Karst. npj Heritage Science, **13** (1), 432, **2025**.
17. WU Y.J., WU Y.J., HE P.R., MENG Q., WANG R.Z., ZHANG M.Y., YUAN G., ZHAO Y., TIAN X. Spatial characteristics of soil potassium in the early stage of vegetation restoration and influencing factors in southwest China's karst region. Scientific Reports, **15** (1), 2106, **2025**.
18. SU Z.M., LI X.K. The types of natural vegetation in karst region of Guangxi and its classified system. Guihaia, (4), 289, **2003** [In Chinese].
19. ZHENG X.J., SHENG M.Y., ZHANG Y., GONG Z.J., WANG L.J. PhytOC sequestration characteristics and phytolith carbon sink potential of karst Masson pine forest in southern China. Science of the Total Environment, **913**, **2024**.
20. SHU Y.G., GONG X.H., WU J.H. Characteristics of soil organic nitrogen fractions under vegetation restoration in karst areas. Scientific Reports, **15** (1), 28180, **2025**.
21. LIN Z.H., LIU C.H., QIN D. Study on ecological sensitivity of Guangxi expressway network planning. Western China Communications Science & Technology, (6), 48, **2022** [In Chinese].
22. TÜRK Y., BODUR M. Assessment and analysis of tree damage caused by forest road construction in a scotch pine stand: a case study from Alabarda/Bolu-Türkiye. Environmental Monitoring and Assessment, **195** (12), 1481, **2023**.
23. JIA X.L., ZHU J.Y., LI Y.Y., WU W.B., HU X.Y. Analysis of the driving role and impact of road construction on carbon stock. Environmental Science and Pollution Research, **30** (25), 67131, **2023**.
24. HAN L.J., HAO X.C. Review on the Environmental Influence of Highway and Prevention Countermeasures. Northern Horticulture, (2), 115, **2011** [In Chinese].
25. YANG S.Q., JIN Z., LUO D., FENG L. Road network expansion and its impact on landscape patterns in the Dongzhi tableland of the Chinese Loess Plateau. Journal of Geographical Sciences, **33** (12), 2549, **2023**.
26. XU H.H. Environmental protection management countermeasures for expressway construction projects under the new situation. Western China Communications Science & Technology, (9), 201, **2021** [In Chinese].
27. LAN X., DU H., SONG T. Q., ZENG F.P., PENG W.X., LIU Y.X., FAN Z.L., ZHANG J.Y. Vegetation carbon storage in the main forest types in Guangxi and the related influencing factors. Acta Ecologica Sinica, **39** (6), 2043, **2019** [In Chinese].
28. LI Y.Q., HE M.Z., JIANG H.J., HUANG J.H., WU Q.B. Biomass and Carbon Storage of Caesalpinia Sappan plantation in Northwest Guangxi. Journal of Fujian Forestry Science and Technology, **47** (4), 22, **2020** [In Chinese].
29. MENG Y.C., GOU R.K., BAI J.K., MORENO-MATEOS D., DAVIS C.C., WAN L.M., SONG S.S., ZHANG H.S., ZHU X.S., LIN G.H. Spatial patterns and driving factors of carbon stocks in mangrove forests on Hainan Island, China. Global Ecology and Biogeography, **31** (9), 1692, **2022**.
30. LI Y., LUO H.F. Spatio-temporal Evolution and Multi-scenario Simulation of Carbon Storage in Karst Regions of Central Guizhou Province:Taking Puding County as An Example. Environmental Science, **45** (2), 961, **2024**.
31. ZHONG R., PU L.J., XIE J.Y., YAO J.M., QIE L., HE G.L., WANG X.Q., ZHANG R., ZHAI J.H., GONG Z.S., LU Y.M., TAO J.W., LI J.G., HUANG S.H. Carbon storage in typical ecosystems of coastal wetlands in Jiangsu, China: Spatiotemporal patterns and mechanisms. Catena, **254**, **2025**.
32. ZHANG J.X., HU R.Z., CHENG X.L., CHRISTOS V., PHILBIN S.P., ZHAO R., ZHAO X.W. Assessing the landscape ecological risk of road construction: The case of the Phnom Penh-Sihanoukville Expressway in Cambodia. Ecological Indicators, **154**, **2023**.
33. YANG S.Q., JIN Z. Impact of road network expansion on landscape ecological risk and soil erosion sensitivity on the Luochuan Tableland of the Chinese Loess Plateau. Regional Environmental Change, **24** (2), **2024**.
34. WEN M.D., ZHANG L.L., WAN H.W., SHI P.R., LU L.H., ZHAO Z.X., ZHANG Z.R., WU J.H. Analysis of Roadside Land Use Changes and Landscape Ecological Risk Assessment Based on GF-1: A Case Study of the Linghua Expressway. Remote Sensing, **17** (2), **2025**.
35. CHEN C., SHI H., MO X., QIU S. Life-cycle water footprint analysis of Bama's biomass fuel in Guangxi combined with environment and economy assessment. Science of the Total Environment, **954**, 176345, **2024**.
36. PENG H., YANG W., NADINE FERRER A.S., XIONG S., LI X., NIU G., LU T. Hydrochemical characteristics and health risk assessment of groundwater in karst areas of southwest China: A case study of Bama, Guangxi. Journal of Cleaner Production, **341**, 130872, **2022**.
37. GAO M., HU Y., BAI Y. Construction of ecological security pattern in national land space from the perspective of the community of life in mountain, water, forest, field, lake and grass: A case study in Guangxi Hechi, China. Ecological Indicators, **139**, 108867, **2022**.
38. HUANG S., TIAN Y.C., ZHANG Q., TAO J., ZHANG Y.L., LIN J.L. Spatiotemporal changes and driving mechanism of ecosystem carbon sink in karst peak cluster depression basin in Southwest Guangxi based on the interaction of "water-rock-soil-air-biology". Ecological Informatics, **83**, 102800, **2024**.
39. BUBIER J., CRILL P., MOSEDALE A., FROLKING S., LINDER E. Peatland responses to varying interannual moisture conditions as measured by automatic CO_2 chambers - art. no. 1066. Global Biogeochemical Cycles, **17** (2), **2003**.
40. CHAVE J., COOMES D.A., BURSLEM D.F.R.P., SIMONSON W.D. Floristic shifts versus critical transitions in Amazonian forest systems. Cambridge University Press, Cambridge, pp. 131-160, **2014**.
41. Beijing Municipal Forestry and Parks Bureau. Technical regulations for accounting and monitoring of forest land carbon sink. Beijing: Beijing Municipal Bureau of market supervision and Administration, China, **2024** [In Chinese].
42. FANG J.Y., LIU G.H., XU S.L. Biomass and net production of forest vegetation in China. Acta Ecologica Sinica, (5), 497, **1996** [In Chinese].
43. ZOU J.W., HUANG Y., ZHENG X.H., WANG Y.S., CHEN Y.Q. Estimation of Net Ecosystem-Atmosphere CO_2 Exchange in Terrestrial Ecosystems Based on the Static

Chamber Method. Chinese Science Bulletin, (3), 258, **2004**.
44. JIANG Z., ZHANG C., LUO W., XIAO Q., WU Z. Research progress and prospect of carbon sink in karst region of China. Carsologica Sinica, **41** (3), 345, **2022** [In Chinese].
45. YIN S.W., GONG Z.W., GU L., DENG Y.J., NIU Y.J. Driving forces of the efficiency of forest carbon sequestration production: Spatial panel data from the national forest inventory in China. Journal of Cleaner Production, **330**, 129776, **2022**.
46. LIU Y., WANG T.J., GAO Y., DANG X.H., WANG J., CHEN Y.N., JIA C.G. Characteristics and distribution pattern of carbon storage variation of the corn farmland ecosystem in the ecotone between agriculture and animal husbandry. Agricultural Research in the Arid Areas, **33** (2), 214, **2015** [In Chinese].
47. HAO Y.L. Impact of expressway construction on vegetation in Sanjiangyuan area. Qinghai Transportation Science and Technology, **33** (4), 34, **2021** [In Chinese].
48. TÓTH G., IVITS E., PROKOP G., GREGOR M., FONS-ESTEVE J., MILEGO AGRÀS R., MANCOSU E. Impact of Soil Sealing on Soil Carbon Sequestration, Water Storage Potentials and Biomass Productivity in Functional Urban Areas of the European Union and the United Kingdom. Land, **11** (6), 840, **2022**.
49. O'RIORDAN R., DAVIES J., STEVENS C., QUINTON J.N. The effects of sealing on urban soil carbon and nutrients. Soil, **7** (2), 661, **2021**.